

RESEARCH

Open Access



Targeting the TDP-43 low complexity domain blocks spreading of pathology in a mouse model of ALS/FTD

Elodie Chevalier^{1†}, Mickael Audrain^{1†}, Monisha Ratnam¹, Romain Ollier¹, Aline Fuchs¹, Kasia Piorkowska¹, Andrea Pfeifer¹, Marie Kosco-Vilbois¹, Tamara Seredenina^{1*}  and Tariq Afroz^{1*}

Abstract

Abnormal cytoplasmic localization and accumulation of pathological transactive response DNA binding protein of 43 kDa (TDP-43) underlies several devastating diseases such as amyotrophic lateral sclerosis (ALS) and frontotemporal lobar degeneration with TDP-43 pathology (FTLD-TDP). A key element is the correlation between disease progression and spatio-temporal propagation of TDP-43-mediated pathology in the central nervous system. Several lines of evidence support the concept of templated aggregation and cell to cell spreading of pathological TDP-43. To further investigate this mechanism in vivo, we explored the efficacy of capturing and masking the seeding-competent region of extracellular TDP-43 species. For this, we generated a novel monoclonal antibody (mAb), ACI-6677, that targets the pathogenic protease-resistant amyloid core of TDP-43. ACI-6677 has a picomolar binding affinity for TDP-43 and is capable of binding to all C-terminal TDP-43 fragments. In vitro, ACI-6677 inhibited TDP-43 aggregation and boosted removal of pathological TDP-43 aggregates by phagocytosis. When injecting FTLD-TDP brain extracts unilaterally in the CamKIIa-hTDP-43NLSm mouse model, ACI-6677 significantly limited the induction of phosphorylated TDP-43 (pTDP-43) inclusions. Strikingly, on the contralateral side, the mAb significantly prevented pTDP-43 inclusion appearance exemplifying blocking of the spreading process. Taken together, these data demonstrate for the first time that an immunotherapy targeting the protease-resistant amyloid core of TDP-43 has the potential to restrict spreading, substantially slowing or stopping progression of disease.

Keywords TDP-43, Spreading, Neuropathology, Immunotherapy, Pathomechanism, ALS, FTD

Introduction

Cytoplasmic mislocalization, misfolding and accumulation of aggregates of transactive response DNA binding protein of 43 kDa (TDP-43) are pathological hallmarks of multiple neurodegenerative diseases including

amyotrophic lateral sclerosis (ALS), frontotemporal lobar degeneration with TDP-43 pathology (FTLD-TDP) [3, 28] and limbic-predominant age-related TDP-43 encephalopathy (LATE) [25]. Moreover, pathological inclusions of TDP-43 have been identified as co-pathologies in Alzheimer's disease (AD), Parkinson's disease (PD) and chronic traumatic encephalopathy (CTE) as well as in rare conditions such as inclusion body myositis (IBM) [9, 16, 24, 33].

Staging of TDP-43 pathology based on *postmortem* analysis of patient brains and spinal cords implies a spatio-temporal spreading of pathology via cell-to-cell transmission that correlates with disease progression [7,

[†]Elodie Chevalier and Mickael Audrain have contributed equally.

*Correspondence:

Tamara Seredenina
tamara.seredenina@acimmune.com

Tariq Afroz
tariq.afroz@gmx.ch

¹ AC Immune SA, EPFL Innovation Park, Building B, 1015 Lausanne, Switzerland



37]. Using a transgenic animal model of TDP-43-driven disease, this process of templated aggregation has been explored [31]. In this study, TDP-43 seeds isolated from FTLD-TDP brains resulted in both local TDP-43 pathology and subsequent spreading throughout the central nervous system in a regional- and time-dependent manner [31]. Recently, seeding and spreading of TDP-43 pathology has been recapitulated using spinal cord extracts from ALS patients in cerebral organoids generated from ALS patient cells [35].

Several lines of evidence point to the importance of the carboxy-terminal (C-terminal) region of TDP-43 in the process of templated aggregation. The C-terminal domain, known as the low complexity domain (LCD), is intrinsically disordered and contains regions enriched in glycine, hydrophobic residues, glutamine and asparagine [2]. While this region of TDP-43 has intrinsic properties to form higher-order physiological assemblies such as stress granules [13], in disease, irreversible inter- and intra-molecular interactions within this region can result in pathologic aggregates [13]. In fact, recent structural and biochemical studies demonstrate that this region adopts a stable protease-resistant amyloid core structure in the ALS and FTD patient brains [4, 5]. Moreover, the disease-specific proteolytic cleavage exposing this amyloid core is shown to further enhance seeding activity important for templated aggregation [19]. Such proteolytic processing of TDP-43 and consequent enrichment of C-terminal fragments in patient brains is a disease-specific signature in addition to other post-translation modifications such as ubiquitination, acetylation, sumoylation or phosphorylation [8, 10, 23, 26, 27, 34]. Recent research assessing both active and passive immunotherapy approaches have confirmed that targeting the C-terminal regions of TDP-43 is essential for efficacy in disease models [1, 6].

Here, we report the creation of a specific mAb, ACI-6677, targeting the protease-resistant amyloid core in the C-terminal region of TDP-43. Using this unique reagent in conjunction with injecting FTLD-TDP brain extracts unilaterally into transgenic mice, spreading of TDP-43 pathology was prevented leading to a decrease of pTDP-43. This work expands our mechanistic understanding of propagation of TDP-43 pathology via extracellular seeding-competent species in the brain and validate the immunotherapy approach for treating disease.

Material and methods

Vaccine design, mouse immunizations and hybridoma generation

Vaccine was engineered by conjugation of recombinant full-length human TDP-43 (Origene) on the surface of SupraAntigen[®] liposomes as described in Afroz et al. [1].

Adult C57BL/6JOLA^{Hsd} or BALB/cOLA^{Hsd} female mice were injected subcutaneously with 200 μ L of vaccines. All animal experiments were approved by the Local Committee for Animal Use and carried out in accordance with cantonal and federal regulations. Animals received six subcutaneous injections at days 0, 4, 7, 21, 35 and 70. Blood samples were collected 7 days before the first immunization (to serve as the baseline control) and at study days 15, 28, 42, 77 and 136. Blood was collected from tail vein into heparin tubes (Microvette Hep-Li CB300 LH Sarstedt ref: 16.443) and mixed by inversion (4 times). After 20 min incubation at 4 °C, samples were centrifuged for 10 min at 21,000 $\times g$ (4 °C), the supernatant (plasma) was collected and stored at -80 °C until further use. Spleens from immunized mice were used. The hybridoma generation (cell fusion partner: PA1 myeloma cell line), subcloning and clone amplification were performed at NanoTools Antikörpertechnik, Germany using proprietary techniques.

Recombinant antibody production

ACI-6677 variable fragment heavy chain (VH) and variable fragment light chain (VL) domains were cloned into mammalian expression vectors containing the mouse kappa constant domain and the mouse IgG2a constant domain, respectively. Chinese hamster ovary cells were transiently transfected with equimolar quantities of heavy and light chain vectors. Antibodies were purified from supernatants by protein A chromatography (mAb select sure, GE Life sciences) followed by sterile filtration. The identity and purity of the purified antibody was confirmed using native and reduced capillary electrophoresis sodium dodecyl sulphate (CE-SDS). Concentrations of antibodies were measured using the NanoDrop Spectrophotometer (Thermo Fisher Scientific).

Enzyme linked immunosorbent assay (ELISA)

For determination of antibody EC_{50} by ELISA, 1 μ g/mL of full length (FL) human recombinant TDP-43 (Selvita) diluted in carbonate bicarbonate buffer (Sigma, SLBQ8494V) pH 9.6 was used to coat ELISA plates (MaxiSorp, Nunc) overnight (ON) at 4 °C. After washing four times with wash buffer (Phosphate buffered saline (PBS)-0.05% Tween-20) and blocking for 1 h at 37 °C with blocking buffer (PBS-0.05% Tween-20 (Merck, 8.22184.0500), 1% bovine serum albumin (BSA, Sigma, A3294)), plates were incubated for 2 h at 37 °C with a concentration range (1000 ng/mL to 0.5 ng/mL) of recombinant antibody ACI-6677 diluted in blocking buffer. Next, plates were washed four times with wash buffer and incubated for 1 h at 37 °C with goat anti-mouse IgG-AP antibody (Jackson, 115-055-164) diluted 1/1000 in blocking buffer. After washing, plates were

incubated for 1 h at room temperature with 1 mg/mL of phosphatase substrate pNPP (S0942, Sigma). The absorbance signal was measured 1 h later at 405 nm wavelength using a plate reader (Tecan Infinity M200).

Epitope mapping was determined by ELISA as described in the previous paragraph with minor changes. FL TDP-43, TDP-43-LCD (expressed in *E. coli*) and selected TDP-43 peptides (custom-made) (Table 1), were diluted in carbonate-bicarbonate buffer at final concentrations of 1 µg/mL for the peptides and of 2.5 µg/mL and 1.3 µg/mL for FL TDP-43 and TDP-43-LCD respectively. After incubation at 4 °C overnight, 4 washes in wash buffer and blocking, ACI-6677 hybridoma supernatant (diluted 50 times in blocking buffer) was incubated on the plate for 2 h at 37 °C.

Surface plasmon resonance

Measurements were performed on a Biacore 8 K instrument (GE Healthcare Life Sciences) with immobilized soluble TDP-43 (Selvita) on a CM5 Series S sensor chip. The instrument was primed with running buffer PBS-P+ and flow cells (Fc) 1 and 2 of channels 1–8 were activated with a fresh solution of 1-Ethyl-3-(3-dimethylamino-propyl) carbodiimide and N-hydroxysuccinimide (EDC/NHS) at 10 µL/min for 420 s. Soluble TDP-43 was diluted in sodium acetate pH 4.5 to a final concentration of 5 µg/mL and injected for 80 s with a flow rate of 10 µL/min on Fc 2. All flow cells were quenched with 1 M ethanol amine at 10 µL/min for 420 s. Prior to analysis, three startup cycles were run. Increasing ACI-6677 mAb concentrations were injected in single-cycle kinetics ranging

from 1.2 to 100 nM, prepared from a threefold serial dilution in running buffer, with a contact time of 300 s and a dissociation time of 3600 s at a flow rate of 30 µL/min. Each cycle was followed by one regeneration using 10 mM Glycine-HCl pH 1.7 with a contact time of 30 s at 10 µL/min, followed by a stabilization period of 300 s. Results obtained from single-cycle kinetics were double-referenced using the blank Fc 1 and a buffer cycle and evaluated using Biacore 8 K evaluation software using the 1:1 kinetic fit model with RI. The following kinetic parameters were obtained: association rate constant (k_a), dissociation rate constant (k_d), affinity constant (K_D) and saturation response (R_{max}). All parameters are reported as mean ± standard deviation (SD).

Human postmortem brain tissues

Human post-mortem tissues were obtained from the brain banks affiliated with the University of California, San Francisco (UCSF), the Queen Square Brain Bank (QSBB) and Netherlands Brain Bank (NBB). Informed consent for autopsy and usage of tissue for research purposes had been obtained from probands or their legal representative in accordance with local institutional review boards. Tissue characteristics are summarized in the Table 2 below.

Immunofluorescence on patient brain sections

The brain samples were cut at 10 µm thickness, mounted on microscope slides and stored at –80 °C until further use. Frozen brain sections were thawed at RT, fixed with 4% paraformaldehyde (PFA) at 4 °C for 15 min and washed 3 times with PBS. Blocking was performed with 5% BSA in PBS-0.25% Triton X-100 for 1 h at RT. The sections were incubated overnight at 4 °C with 1 µg/mL and 5 µg/mL of primary antibody ACI-6677 and pTDP-43 (s409/410) (Biolegend, 829901) respectively diluted in 2.5% BSA in PBS-0.25% Triton X-100. The next day, the sections were washed 3 times with PBS prior to the addition of Alexa Fluor-633-labeled goat anti-rat and Alexa Fluor-488-labeled goat anti-mouse antibodies diluted 1/500 in PBS. Secondary antibodies were incubated for 30 min at RT. After three washes with PBS, 0.1% Sudan

Table 1 Protein and peptide used for epitope mapping

Proteins/peptides	TDP-43 coverage (amino acid position)
FL TDP-43	1–414
TDP-43 LCD	274–414
Peptide 1	254–320
Peptide 2	340–390
Peptide 3	389–414

Table 2 Human post-mortem CNS tissue

Case #	Brain bank	Disease	Purpose
1	UCSF	FTLD-TDP Type A	Immunolabeling on tissue section
2	QSBB	FTLD-TDP Type A	Cell-based seeding assay, in vivo study, Western Blot
3	NBB	Non-demented control	Cell-based seeding assay (control)
4	NBB	FTLD-TDP Type A	Limited proteolysis

Black dissolved in 70% ethanol was added to the brain sections for 15 min at RT to minimize auto-fluorescence. After three washes in PBS, Prolong Antifade Reagent with 4',6-Diamidino-2-phenylindol (DAPI) was added and the sections were mounted with coverslips. The brain sections were dried in the dark and imaged with the Panoramic 150 Slide Scanner using the fluorescein isothiocyanate (FITC), Cy5 and DAPI channels.

Western blot

Western blotting (WB) was performed on sarkosyl-insoluble extracts prepared as described previously [21] from human brains of cases with FTLTDP type A pathology and on sarkosyl-insoluble extracts which underwent a limited proteolysis [5]. Briefly, sarkosyl-insoluble samples were treated with 0.4 mg/mL pronase (Sigma, 10165921001) for 1 h at 21 °C, then centrifuged at 20,000 g for 30 min at 4 °C. Supernatant was discarded and pellet was resuspended in PBS by sonication with a sonicator probe (Q-Sonica) 30 times at amplitude 30.

Sarkosyl-insoluble extracts were mixed with 4x Sample Loading buffer and 0.1 mM Dithiothreitol (DTT) and boiled for 10 min at 95 °C. The samples were loaded on a 4–12% Bis–Tris gel and migrated at 100 Volt (V) for 90 min. The proteins were transferred on a nitrocellulose membrane using the iBlot 2 system (20 milliamperes (mA), 7 min). The membrane was blocked for 1 h at RT under agitation in LI-COR® blocking buffer. Primary antibodies (ACI-6677, anti-pS409-410 TDP-43 (Biolegend, 829901) and anti-TDP-43 (Proteintech, 60019-2-Ig)) were diluted 1/1000 in PBS-0.1% Tween-20/LI-COR® blocking buffer (1:1) and incubated on the membrane overnight at 4 °C under agitation. The membrane was washed 3 times in PBS-0.1% Tween-20 under agitation. Secondary antibodies donkey anti-mouse IRDye680CW and donkey anti-rat IRDye800CW (LI-COR®) were diluted 1/10,000 in the same buffer as the primary antibodies and the membranes were incubated for 1 h at RT under constant agitation. The membranes were scanned after 3 washes in PBS with 0.1% Tween-20 using LI-COR® Odyssey imager.

TDP-43 aggregation assay in vitro

C-terminally fused maltose binding protein to recombinant TDP-43 (TDP-43-MBP), containing a Tobacco Etch Virus (TEV) protease cleavage site, was produced in *E. coli*, aliquoted and stored at -80 °C (Selvita). For each experiment, fresh aliquots of TDP-43-MBP were quickly thawed at RT and kept on ice afterwards. Storage buffer was exchanged against assay buffer (30 mM Tris, 150 mM NaCl, pH 7.4) using centrifugal filters and the protein concentration was determined by ultraviolet (UV) spectroscopy at 280 nm (NanoDrop).

TDP-43-MBP was diluted in assay buffer to a final concentration of 2.5 μM and mixed with 2.5 μM ACI-6677 or isotype control (IgG2a mAb) in low binding tubes. Aggregation was induced by addition of TEV protease at a final concentration of 10 μg/mL in 96-well plate with 80 μL final volume per well. Aggregation was monitored by absorbance measurement at 600 nm in the center of the well every 15 min with 5 s shaking before each measurement over 24 h in technical triplicates. The plate was constantly kept in the plate reader at 25 °C and sealed with foil. To confirm complete cleavage of TDP-43-MBP by TEV protease in the presence of mAbs, samples were analyzed at 24 h by capillary electrophoresis (JESS, ProteinSimple). Samples were mixed with 5X Mastermix using ProteinSimple protocol and analyzed in a Separation Module. An anti-C-terminal TDP-43 antibody [1] labelled with DyLight680 was used as detection at 20 μg/mL.

TDP-43 aggregates uptake by mouse primary microglia

TDP-43 aggregates were generated using recombinantly produced His-SUMOStar-Flag tagged full length TDP-43. The soluble His-SUMOStar-Flag-TDP-43 was purified by affinity chromatography followed by His-SUMOStar cleavage and removal by size exclusion chromatography. To induce aggregation the resulting Flag-TDP-43 protein was incubated at RT for 7 days prior to centrifugation at 20,000 g for 30 min at 4 °C. The pellet containing fibrils was resuspended in PBS pH 7.4. To confirm presence of fibrillar structures, the TDP-43 aggregates were analyzed by negative stain transmission electron microscopy (nsTEM). In brief, 3 μL of sample was applied onto a hydrophilized EM grid, washed with water, and negatively stained using 2% uranyl acetate. The grid was imaged using a FEI Tecnai G2 Spirit Biotwin electron microscope run at 100 kV accelerating voltage.

Microglial uptake experiments were performed as described previously [1]. Briefly, mouse primary microglia were plated at 30,000 cells per well in growth medium and incubated for 48 h at 37 °C 5% CO₂ in a humidified atmosphere. Immune complexes were prepared in basal medium at 2X final concentration by mixing pHrodo™ labelled TDP-43 aggregates and antibodies in a dilution plate (Eppendorf 96-well sterile) and incubating overnight at 4 °C. The dilution plate was equilibrated at RT while the cells were washed three times with basal medium. After the final wash, 100 μL of basal medium remained on the cells to which 100 μL of pHrodo™ labelled TDP-43 aggregates from dilution plate was added. Cells were immediately placed inside the automated microscope (Incucyte ZOOM) for live imaging of phase contrast and green fluorescence for 24 h.

Pharmacokinetics (PK)

The *in vivo* PK study was approved by the Institutional Animal Care and Use Committee (IACUC) of WuXi AppTec and performed in an accredited animal facility. The nine female C57BL/6 J mice (age: 7–11 weeks) used in this study were purchased from Lingchang/Vital River Laboratory Animal Co., Ltd., Shanghai/Beijing, P.R. China. Mice were acclimated with free access to food and water for at least 3 days before the treatment. ACI-6677 (vehicle: 10 mM PBS (pH 7.4), clear solution) was administered as a single intraperitoneal (i.p.) injection at 60 mg/kg. Mice were administered antibody based on their body weight measured on the day of antibody administration.

Blood samples were collected from saphenous vein at the following time-points: 0.25, 1, 8, 24, 72, 168, 240, 336, 504, 672 h from 3 respective mice per time point., except at 72 h where 6 mice were sampled. All blood samples were transferred into precooled vials containing EDTA-K₂ and kept on ice. Blood samples were processed for plasma within 15 min after collection, by centrifuging at 4 °C, 3200 g for 10 min. Approximately 20 µL of plasma was collected into pre-labeled polypropylene tubes. All aliquots were stored at –60 °C until further ELISA analysis was performed. Concentrations of all plasma samples were back-calculated against a reference standard using a non-linear 4-parameter regression fit including a 1/y² weighting. Antibody concentration–time profiles in plasma were used to calculate the pharmacokinetics (PK) parameters of ACI-6677 in mouse by Non-Compartmental Analysis (NCA) (Phoenix WinNonlin 6.3, Certara®).

Characterization of FTLD-TDP brain extracts

Human sarkosyl-insoluble extracts were prepared as described in Laferriere et al. [21]. Resulting extracts were characterized by western blot as described above using anti-TDP-43 (Novus, NBP1-92695) and anti-pS409-410 TDP-43 (Biolegend, 829901) antibodies to detect total and phosphorylated forms of TDP-43 in sarkosyl-insoluble brain extracts. The extracts were evaluated for their seeding capacity in a cell based seeding assay as described previously [31]. In brief, doxycycline (DOX) inducible iGFP-NLSm cells (Porta et al. [31]) were transduced with the FTLD-TDP sarkosyl-insoluble brain extract using Ab-DeliverIN™ (AI21000, OZ Biosciences). Ab-DeliverIN™ (0.5 µL per well of a 96-well plate) was pre-mixed with the extracts and incubated for 15 min at RT. Seventeen microliters of OPTIMEM per well were added onto the mix. Twenty microliters of the reaction were added in each well and incubated for 4.5 h at 37 °C, 5% CO₂ in humidified atmosphere. The media was exchanged for culture media containing 1 µg/mL DOX. Three days after transduction of the extracts, cells were

fixed using 4% PFA. Cells were further labelled with anti-pS409-410 TDP-43 antibody (Biolegend, 829901, 2 µg/mL) and incubated overnight at 4 °C after blocking for 1 h at RT. Secondary antibody were incubated for 1 h at RT and washed with PBS prior to imaging the cells using InCell Analyzer 2200.

In vivo efficacy study in CamKIIa-hTDP-43NLSm transgenic mice injected with FTLD-TDP brain extracts

In-life phase

In vivo efficacy study was performed as previously described in Afroz et al. [1] with minor changes. Double transgenic CamKIIa-hTDP43NLSm animals were generated by crossing hemizygous females (JAX Stock # 14650: B6;C3-Tg(tetO-TARDBP*)4Vle/J) with hemizygous males (JAX Stock # 007004: B6.Cg-Tg(CamKIIa-tTA)1Mmay/Dbo). Based on power calculations for histological neuropathology evaluation from other models of neurodegeneration, a group size of n=8–10 was predicted. Additionally, to ensure this number for the final analysis and to allow for a 60–70% success rate of stereotaxic surgery and inoculation of patient brain extracts, the initial group size was defined as n=15 per treatment group. A total of 52 mixed gender mice were used in this study. All breeders and mice were kept on 200 mg/kg DOX diet until 12.5 ± 2 weeks of age. At 13.5 ± 2 weeks, CamKIIa-hTDP43NLSm mice were anesthetized with buprenorphine at 1 mg/kg and immobilized in a stereotaxic frame. Human sarkosyl-insoluble extracts were sonicated prior injection in the dorsal hippocampus. Each injection site (needle introduced in the left hemisphere following Bregma coordinate: –2.0 mm anterior and left 1.3 mm from midline; three dorsal hippocampus location with initial depth of –1.95 mm below the dura and then partially withdrawing the needle to –1.55 mm for the second injection and again to –1.15 mm for the final injection) received 1 µL of sarkosyl-insoluble human brain extract (3 µL per mouse) at a rate of 0.3 µL/min. One day later, weekly i.p. injection of mAbs (60 mg/kg) started, for 13 consecutive weeks. Two antibodies were tested: ACI-6677 and isotype control (IgG2a). Terminal collection was done 13 weeks post injection and one day after final dose administration.

Behaviour assessment

Animals were weighed at day 0 and then weekly for the duration of the study. Motor performance was assessed weekly for signs of motor dysfunction, including tremor and claspings. Each sign was scored on a scale of 0–3: normal (no dysfunction) (0), mild (1), moderate (2) or severe (3) dysfunction.

Embedding and sectioning

Brain hemispheres subjected to histology were snap frozen and then immersion-fixed in formalin for 24 h. The tissue was then embedded into optimal cutting temperature (OCT) matrix and frozen on dry ice with a super-cooled bath of 2-methylbutane. Frozen tissue blocks were sectioned coronally at 20 μm thickness per section. Slides were stored at -20°C prior to immunofluorescence (IF) staining.

Immunofluorescence (IF)

Staining was performed on a Leica BOND-RX in accordance with Biospective Standard Operating Procedures. For the dual pTDP43/Neuronal Nuclear protein (NeuN) IF staining, the slides initially underwent a fixation/permeabilization step in Methanol/Acetone (1:1) for 10 min and washed in PBS. Then epitopes were retrieved in Leica ER1 buffer pH6 (AR9640) for 10 min at 100°C , followed by an incubation with Protein Block (Power-Vision IHC/ISH Super Blocking, Leica, Ref. PV6122). Slides were then incubated with primary antibodies in two steps, first with anti-pS409-410 TDP43 (Biolegend, 829901, Rat mAb, 1/500), followed by anti-NeuN (Millipore, MAB377(CH), Mouse Ab, 1/500). Next, secondary antibodies were incubated in two steps, firstly with a mix of antibodies: anti-mouse-Cy3 (Jackson, Goat Ab, 1/200) and anti-Rat-biotin (Jackson, Goat Ab, 1/250), and secondly with Streptavidin-Cy5 (Jackson, 1/300). Finally, slides were incubated with DAPI (1/300). All antibodies were diluted in BOND antibody diluent (AR9352) and slides were mounted in antifade and cover slipped.

Imaging and image analyses

The IF slides were digitized using an Axio Scan.Z1 digital whole slide scanner (Carl Zeiss, Canada). Region of interest (ROIs) were delimited using a U-Net convolutional neural network trained on a dataset of manually painted tissue sections. The ROIs then underwent visual QC review, and were manually adjusted, if needed. Quantification of IHC staining (% area stained) was performed

on each of the digitized slides using Biospective's PERMITS™ process. Additionally, colocalization of pTDP-43 and NeuN was calculated from the segmented images. The IF analysis and quantification was performed in a blinded manner with respect to cohort.

Statistics

Graphs represent mean \pm SD or SEM for in vitro and in vivo experiments respectively. For statistical analysis of the percentage inhibition of aggregation and TDP-43 uptake by microglia, a ratio paired t-test was performed between the ACI-6677 group and the isotype control group. For TDP-43 uptake by microglia, data from 3 independent experiments with 6 technical replicates were normalized to the no mAb control in each experiment. For TDP-43 aggregation assay, data from 2 independent experiments with 3 technical replicates were normalized to isotype control after blank subtraction (isotype control without TEV protease). For statistical analysis of the in vivo study, ordinary one-way ANOVA was performed with Tukey's correction for multiple comparison. Significance (two-tailed) is reported at $*p < 0.05$, $**p < 0.01$, $***p < 0.001$ and $****p < 0.0001$. For correlation analysis, 2 data points were excluded due to mAb exposure measurement below the quantification limit of the assay (ELISA). Correlation parameters were computed using Pearson correlation (r^2 : coefficient of determination and p-value).

Results

ACI-6677 binds with high affinity to protease-resistant amyloid core of TDP-43

The mAb, ACI-6677, was identified from a panel of anti-TDP-43 mAbs obtained using the SupraAntigen® platform post immunization of mice [1]. ACI-6677 bound full-length TDP-43 with an EC_{50} of 63 pM (Fig. 1A) and a K_D of 380 pM (Fig. 1B) measured by ELISA and surface plasmon resonance (SPR), respectively. Epitope mapping using an ELISA on peptides covering the C-terminal sequence of TDP-43, demonstrated binding of ACI-6677

(See figure on next page.)

Fig. 1 ACI-6677 binds with high affinity to the low complexity domain of TDP-43. **A** The binding of ACI-6677 to human TDP-43 was measured by ELISA and **B** measured by SPR; blue line depicts the experimental data and black line depicts the data fit to the model; **C** Epitope mapping of ACI-6677 using various peptides derived from the human TDP-43 sequence (coverage indicated by a bar above the cartoon of the TDP-43 domains) indicates binding to the LCD and to peptide 1 (aa 254–320); NTD, N-terminal domain; RRM, RNA Recognition Motif; LCD, Low Complexity Domain; **D** Immunoblotting with ACI-6677 or two control antibodies, an anti-total TDP-43 mAb and an anti-pTDP-43 (specific for pS409/pS410) mAb, on sarkosyl-insoluble brain extracts prepared from frontal cortex of cases with FTLD-TDP type A before (–) or after (+) limited proteolysis (revealing the protease resistant fragments) to determine the binding of ACI-6677 to pTDP-43, TDP-43, C-terminal fragments (CTFs) and the protease resistant fragments. Bottom panels with enhanced contrast included to show the binding to protease resistant fragments; molecular weight (kDa) markers shown on the left; **E** Immunolabeling with ACI-6677 (green), an anti-p-TDP-43 mAb (red) and DAPI (cell nuclei, blue) demonstrates binding of ACI-6677 to pTDP-43 (arrowheads) in sections from a FTLD-TDP type A patient (temporal cortex). Arrows indicate areas of physiological nuclear TDP-43. Scale bar = 20 μm

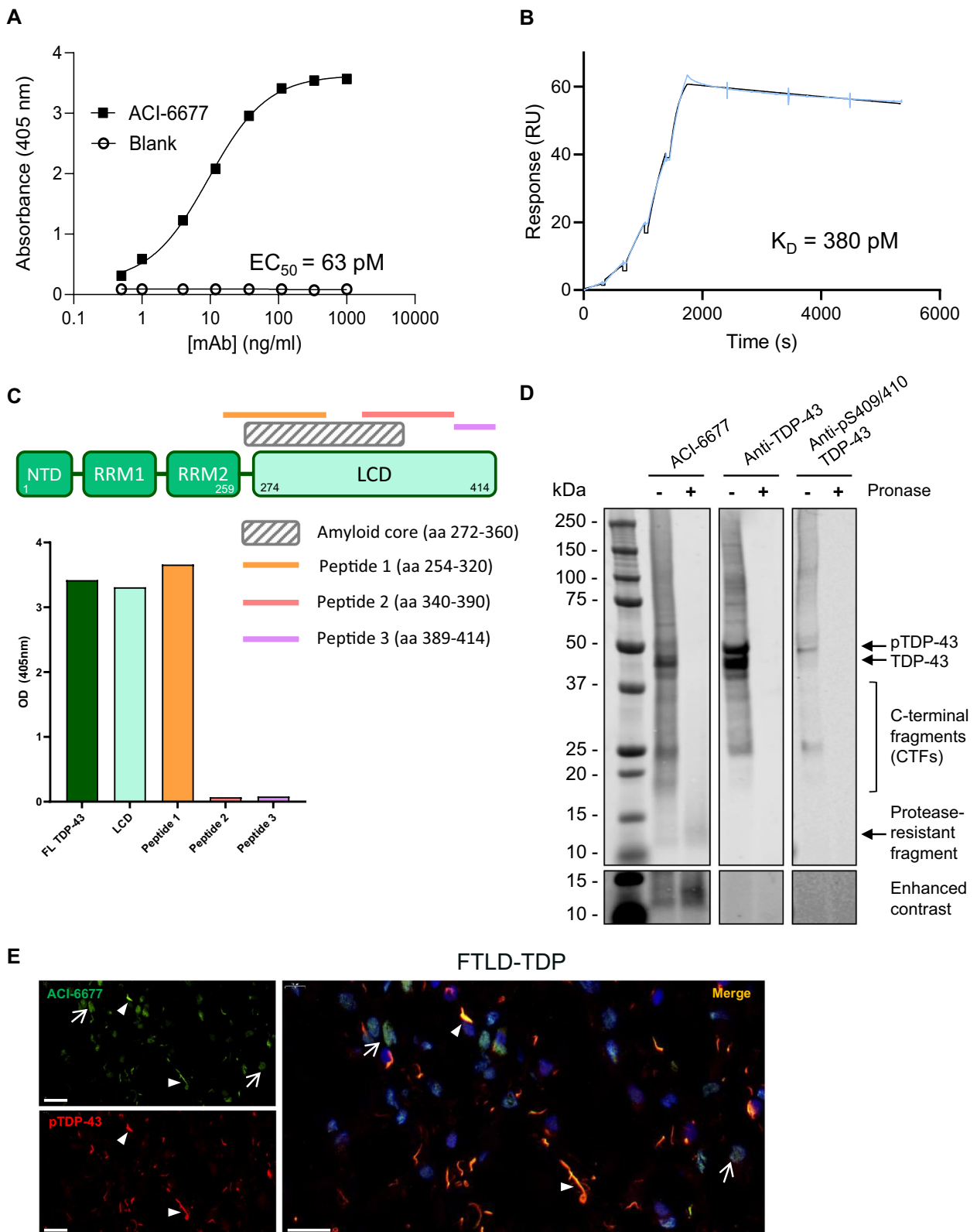


Fig. 1 (See legend on previous page.)

to peptide 1 from 254 to 320 and to the LCD from 274 to 414 whereas no binding was shown to peptide covering amino acids 340 to 414. By combining these data, it can be deduced that ACI-6677 binds within the region 274–320. This epitope lies within the C-terminal region (272–360) harboring protease-resistant amyloid core in patient brains [4, 5] (Fig. 1C).

Immunoblot of FTLD-TDP type A sarkosyl-insoluble brain extracts revealed binding to C-terminal fragments in addition to the band at 43 kDa corresponding to full-length TDP-43 (Fig. 1D). Furthermore, using a control antibody binding to the phosphorylated TDP-43 epitope, pS409/410, we confirmed that ACI-6677 binds to similar molecular weight (MW) bands of C-terminal fragments retaining disease-specific phosphorylation sites (Fig. 1D). In addition, limited proteolysis of the sarkosyl-insoluble FTLD-TDP type A brain extract revealed that ACI-6677 binds to the resulting protected 12 kDa core of TDP-43 (Fig. 1D enhanced contrast panels, Fig. S1). As expected, following limited proteolysis, the antibodies binding either proximal to the low complexity domain (TDP-43 mAb binding in RRM2 region) or extreme C-terminal (pS409/410 TDP-43 mAb) regions did not show a signal on immunoblots (Figs. 1D and S1).

ACI-6677 labels pathological TDP-43 in postmortem disease brain tissue

Using sections from the temporal cortex of a case with FTLD-TDP type A pathology, pTDP-43 was localized using the anti-p409/410 mAb (Fig. 1E). Incubating the sections with ACI-6677 revealed binding to neuronal cytoplasmic inclusions and dystrophic neurites colocalizing with the pTDP-43 labeling (Fig. 1E, arrowheads). In addition, ACI-6677 labeled non-phosphorylated TDP-43 in the nucleus (Fig. 1E). Together, these data confirmed in situ target engagement of TDP-43.

ACI-6677 inhibits TDP-43 aggregation in vitro

The ability of ACI-6677 to block TDP-43 aggregation was assessed in vitro. ACI-6677 or an isotype control were mixed with TDP-43-MBP prior to MBP cleavage by TEV protease to induce aggregation of TDP-43 which was followed by measuring the optical density of the solution at 600 nm. A capillary electrophoresis was performed on the same samples at the end of the experiment to ensure that aggregation inhibition was measured in this assay and not inhibition of TEV protease cleavage (Fig. S2A). ACI-6677 or the isotype control did not interfere with TDP-43-MBP cleavage which resulted in only one band corresponding to TDP-43 as compared to the higher molecular weight band observed when TEV protease was not used on the TDP-43-MBP sample. ACI-6677 completely inhibited TDP-43 aggregation at an equimolar

TDP-43-to-mAb ratio (Fig. 2A and B). The effect was indistinguishable from the result without aggregation induction (i.e., without TEV protease cleavage; Fig. 2A and B). The percentage of inhibition by ACI-6677 was 97% when normalized with an isotype control antibody (Fig. 2B).

ACI-6677 potentiates uptake of TDP-43 aggregates by mouse microglia

Enhanced uptake and therefore clearance of the pathological protein via formation of immune complexes and engagement of Fc-gamma receptors expressed by phagocytic cells is an anticipated contributing mechanism for efficacy in vivo. Therefore, the ability of ACI-6677 to engage phagocytic cells to clear TDP-43 aggregates by Fc gamma receptor-dependent mechanisms was evaluated. For this, an in vitro assay using mouse primary microglia was utilized. Antibodies were complexed with pHrodo-labeled aggregated TDP-43 which contained fibrillar structures (Fig. S2B) prior to addition on the mouse primary microglia. Internalization of the immune complexes by microglia was monitored over 24 h by following pHrodo fluorescence. As compared to the level of internalization using either TDP-43 aggregates alone or in the presence of an isotype control mAb, a significant threefold increase in the uptake of labeled TDP-43 aggregates was observed in the presence of ACI-6677 (Figs. 2C and S3). The kinetics of uptake of immune complexes increased over time with the maximum achieved between 5 and 10 h (Fig. 2C and D). These data highlight the role of Fc-mediated phagocytosis to maximize the therapeutic activity of ACI-6677.

Systemic treatment with ACI-6677 reduces pathological TDP-43 spreading in vivo

As the epitope of ACI-6677 is in the amyloid core and the mAb potentially inhibited aggregation of TDP-43 in vitro, the ability of ACI-6677 to modulate pathology in vivo was assessed using the CamKIIa-hTDP-43NLSm mice inoculated with FTLD-TDP type A brain extracts. This model, in which the mice are injected in one hemisphere only, allows evaluation of both the generation of pTDP-43 in brain tissue as well as modulation of spreading to the contralateral side in vivo.

In order to support the dosing paradigm to be used, a single-dose PK study was performed in wild type mice. ACI-6677 demonstrated an excellent sustained exposure in blood with a half-life of 17 days following intraperitoneal administration at 60 mg/kg (Fig. S4A). No adverse effects were observed over 28 days supporting the safety of the mAb for targeting TDP-43 in vivo. Based on the observed half-life, a weekly intraperitoneal dosing regimen at 60 mg/kg was selected (Fig. S4B).

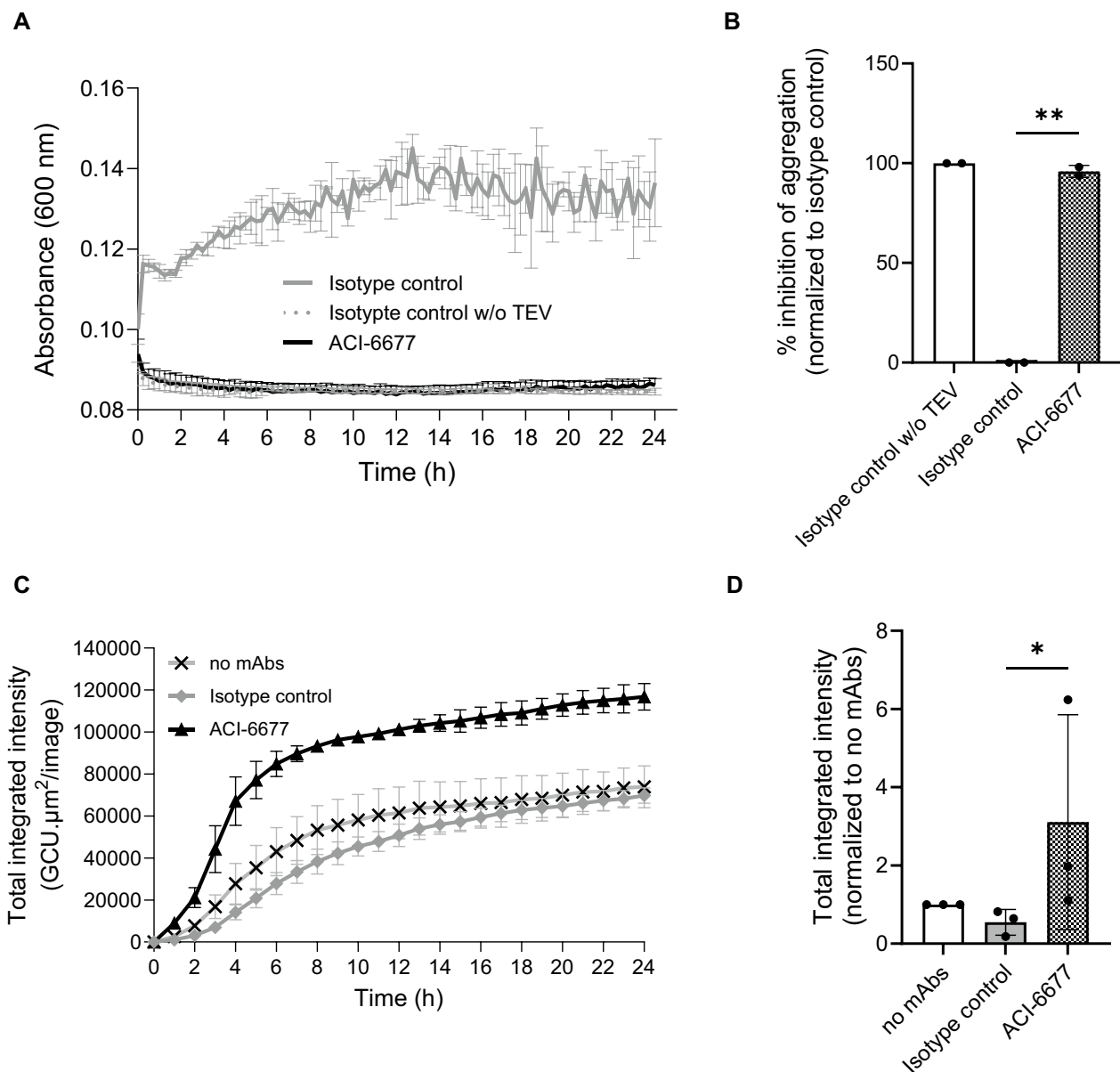


Fig. 2 ACI-6677 inhibits human TDP-43 aggregation and promotes phagocytic clearance by microglia. **A** *de novo* aggregation was assessed using 2.5 μM of ACI-6677 in an assay where the TEV protease is added to cleave MBP-tagged TDP-43, initiating the aggregating process. An isotype control mAb in the presence or absence of the TEV protease provides the kinetic profiles for maximal or no aggregation, respectively; Data represent mean \pm SD of 3 independent replicates. **B** Quantification of percent aggregation inhibition at 24 h from 2 independent experiments normalized to the isotype control without TEV protease. Data shown as mean \pm SD reported using a ratio-paired t-test $**p < 0.01$; **C** Phagocytosis assay with mouse microglia of ACI-6677-TDP-43 immune complexes over 24 h; the total integrated intensity (expressed as green calibrated unit (GCU) \times mm^2 per image) of fluorescent pHrodoTM-labeled TDP-43 (30 nM) internalized at each timepoint is reported after incubation with 30 nM of ACI-6677 or isotype control mAb. Data represents mean \pm SD from three technical replicates; **D** Quantification of total integrated intensity at 6 h from three independent experiments normalized to the no mAbs control. Data shown as mean \pm SD reported using a ratio-paired t-test $*p < 0.05$

Prior to inoculation, the FTL-D-TDP type A brain extracts were characterized for the presence of aggregated pTDP-43 by immunoblot (Fig. S5A) and ability to induce templated-aggregation of TDP-43 in a cell-based model of TDP-43 seeding [31] (Fig. S5B). In this assay, the

extract was transduced to the cells using a protein delivery reagent prior to DOX addition to induce hTDP-43-NLSm-GFP. After 3 days, colocalization of GFP-tagged TDP-43 with pTDP-43 was assessed and demonstrated that these cells developed pathological aggregates when

transduced by the FTLN-TDP brain extracts as compared with a control (Fig. S5B). These data confirmed the seeding capacity of the brain extracts validating their use to induce pathology in the mouse model to evaluate spreading.

Following doxycycline removal to induce the transgene expression, CamKIIa-hTDP-43NLSm mice were stereotactically injected with the FTLN-TDP type A brain extracts described above in the dorsal hippocampus and treated with ACI-6677 or an IgG2a isotype control starting 24 h after inoculation to allow the assessment of therapeutic paradigm (Fig. S4B). Thirteen weekly injections of ACI-6677 or the isotype control mAb resulted in steady state plasma exposures measured at terminal time points (1787 $\mu\text{g/mL}$, Fig. S6A). Assuming 0.1% blood to brain penetration [18], the predicted exposure of ACI-6677 in the brain ($\approx 1787 \text{ ng/mL}$) would be ≈ 30 fold higher than the measured K_D of ACI-6677 (380 pM or 57 ng/mL). In this study, no differences in behavior, as assessed by tremor and clasping measurement, were observed between the groups (Fig. S6B–D) similar to what was previously reported by Porta et al. [31].

On the cellular level, pTDP-43 pathology was observed in the hippocampus 3 months post-injection (mpi) with substantial pathology in the ipsilateral and contralateral sides compared to non-inoculated mice (no extracts) confirming propagation of pathology (Fig. 3A, upper and middle panel). On the ipsilateral side at 3 mpi, pTDP-43 pathology was significantly induced in mice receiving the isotype control compared with non-inoculated mice (Fig. 3B). In the ACI-6677 treatment group, a significant reduction in pTDP-43 pathology (by 51%) was observed compared with the isotype control group (Fig. 3B).

The significant increase in pTDP-43 pathology on the contralateral side in mice administered with isotype control as compared with non-inoculated mice confirmed a robust spreading of pathology from ipsi- to contralateral hippocampus. In mice treated with ACI-6677, a significant reduction (i.e., 61%) in pTDP-43 pathology was observed at the contralateral side compared with the isotype control group (Fig. 3C). These data confirmed the ability of the mAb to substantially neutralize the TDP-43

seeding species and prevent their transmission and templated aggregation. When correlating the amount of pTDP-43 pathology in the ipsilateral and contralateral sides with the antibody exposure, a negative correlation was observed confirming the exposure–response relationship (Fig. 3D).

Discussion

Immunotherapy is an attractive, clinical approach to target neurodegenerative diseases driven by TDP-43 as the mechanism involves inhibiting extracellular propagation of the underlying pathological seeds via neutralization as well as immune mediated elimination via mAbs [1]. Thus, for successful targeting of TDP-43, identifying the amino acid regions involved in propagation and seeding of pathology is essential to define the optimal epitopes for therapeutic targeting. Importantly, as antibodies act in the extracellular compartment of tissues, immunotherapy does not alter the physiological, homeostatic role of TDP-43 (Afroz et al. [1]), offering a safe means to target the pathological forms of such a crucial protein.

In TDP-43 proteinopathies, the C-terminal region of the protein is of particular interest for several reasons. First, *postmortem* analyses show the enrichment of truncated C-terminal fragments in the detergent insoluble brain extracts and is considered a pathological hallmark [26, 28] in contrast to minimal accumulation of N-terminal domains [20]. Second, recently described high-resolution structures of the C-terminal region of TDP-43 from patient brain extracts demonstrate the presence of a protease-resistant amyloid core involved in TDP-43 aggregation [4, 5]. Third, TDP-43 antibodies targeting the low complexity domain demonstrate efficacy in models of ALS/FTD [1, 32]. In this report, we show that the amyloid core region of TDP-43 can be successfully targeted by a mAb to efficiently block the propagation of TDP-43 pathology in a transgenic mouse model of ALS/FTD. This data validates the mechanism of action of immunotherapy in TDP-43 proteinopathies and further supports targeting the low complexity domain with mAbs to achieve functional efficacy [1, 32].

(See figure on next page.)

Fig. 3 ACI-6677 reduces spreading of TDP-43 pathology in CamKIIa-hTDP-43NLSm transgenic mice inoculated in one hemisphere with FTLN-TDP-derived brain extracts. **A** Immunohistochemistry post 13 weeks of treating the CamKIIa-hTDP-43NLSm mice with ACI-6677 (bottom), the isotype control mAb (middle) or untreated mice (top, no extracts) was performed using an anti-pTDP-43 mAb (red) and anti-NeuN mAb (yellow); the ipsilateral and contralateral hippocampal regions are indicated and representative low and high (scale bar = 40 μm) magnification provided; **B, C** Quantification of the level of pTDP-43 (mean staining density) in the ipsilateral (**B**) and contralateral (**C**) hippocampi of ACI-6677 (n = 13) versus isotype control (n = 14) treated mice; background level of pathology in transgenic mice ("no extracts", n = 8) injected in the hippocampus with PBS and not treated with antibodies is provided. Data represent mean \pm SEM. A one-way ANOVA followed by a Tukey post-hoc test for multiple comparisons was used. ** $p < 0.01$; *** $p < 0.001$; **** $p < 0.0001$; **D** Correlation of the pTDP-43 levels with the concentration of ACI-6677 (measured in plasma 24 h post the last dose) for the ipsilateral ($r^2 = 0.37$ and $p = 0.06$) and contralateral ($r^2 = 0.23$ and $p = 0.17$) regions

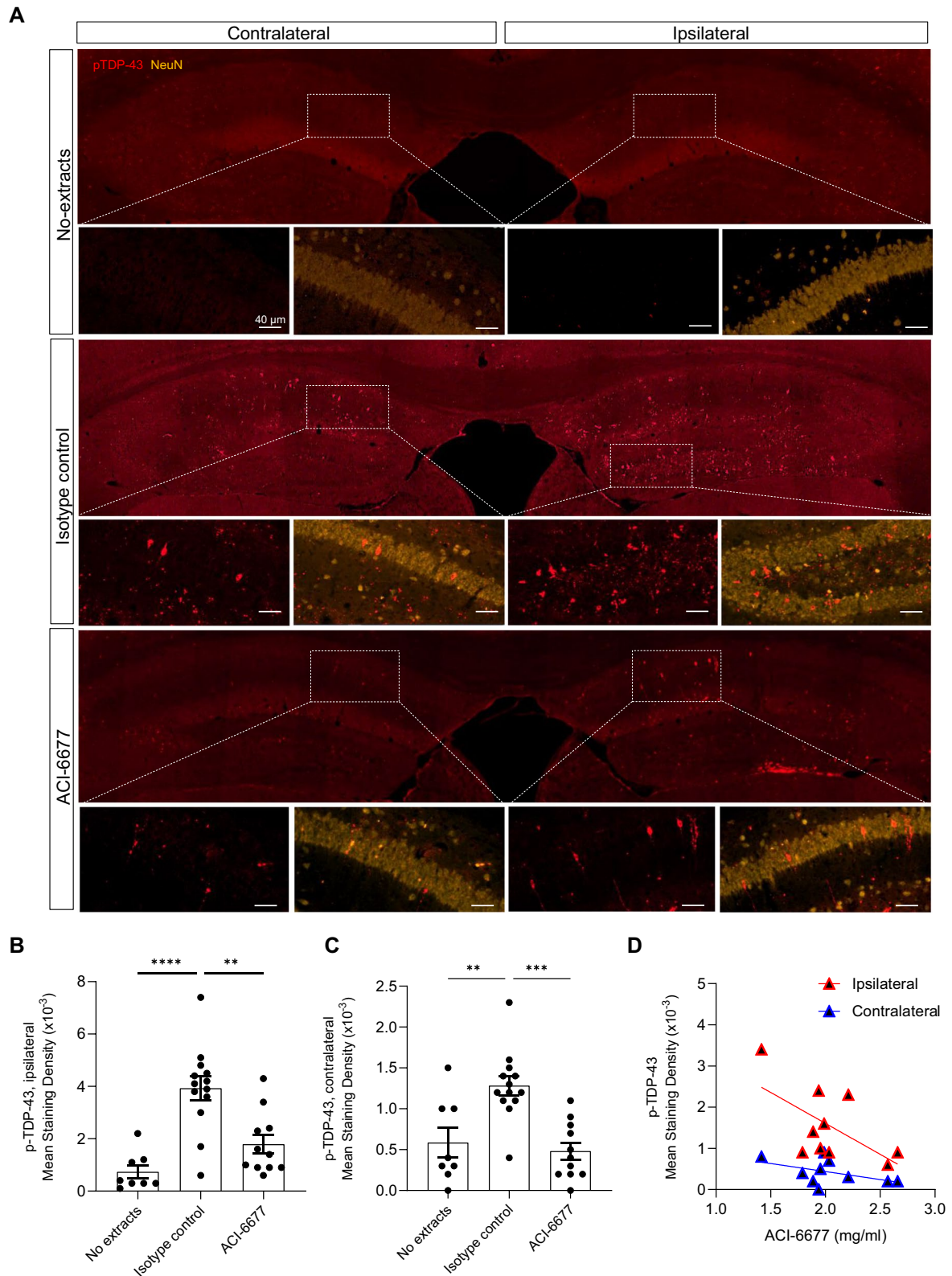


Fig. 3 (See legend on previous page.)

Our data shed light on the identity and nature of pathogenic C-terminal species present in patient brains. ACI-6677 epitope mapping confirmed its binding to the amyloid core region present in patient brain extracts. This was further corroborated by immunoblot where ACI-6677 bound the C-terminal fragments in sarkosyl-insoluble brain extracts following limited proteolysis. Interestingly, in both brain insoluble fractions and patient brain sections, all species recognized by ACI-6677 were also bound by an antibody specific to pS409/410, suggesting that the extreme C-terminal region harboring the disease-specific phosphorylation sites is retained in fragments containing the amyloid core. This was confirmed by immunofluorescence on patient brain sections, where the signal of ACI-6677 colocalized with pTDP-43 signal, demonstrating target engagement of ACI-6677 to pathological TDP-43.

The availability of an antibody binding in the amyloid core of TDP-43 opens new avenues for biochemical, ultrastructural, and neuropathological characterization of TDP-43 pathology to obtain further insights into disease mechanisms and classification. Currently, neuropathological stratification of TDP-43 subtypes is only based on the combination of morphology and localization of inclusions and the specific immunoblot pattern of C-terminal fragments in the sarkosyl-insoluble brain fractions [22, 36]. As ACI-6677 bound in the protease-resistant core of TDP-43 in FTLTDP type A extracts, it would be interesting to evaluate its potential for *postmortem* disease stratification by assessing the relative size of the protease-resistant cores in various TDP-43 subtypes. Even though the majority of the amino acid sequence in the amyloid core region is conserved in TDP-43 pathology subtypes, differences at the N and/or C-terminus of this region, as demonstrated by the amyloid core structures from TDP-43 subtypes A [4] and B [5], may underlie the observed differences in seeding potency of brain extracts from various TDP-43 subtypes [30, 31].

The elucidation of high-resolution structures of the low complexity domain of TDP-43 has expanded the mechanistic understanding of the role of this region in pathobiology [5, 19]. This region of TDP-43, intrinsically disordered and demonstrated to contain little secondary structure in native state [11], adopts a stable amyloid structure in patient brains [4, 5]. Even though the molecular mechanisms leading to these structural transitions are not clear, it is evident that this amyloid containing region can serve as a nucleation site resulting in further maturation of existing aggregates and propagation of pathology [19]. Kumar et al. [19] demonstrated that proteolytic processing of recombinantly produced TDP-43 fibrils exposes this nucleation site to boost its seeding activity in an *in vitro* model of seeded aggregation. This is

in line with the previous data demonstrating that limited proteolysis retains the seeding activity of patient-derived brain extracts *in vitro* [29]. Importantly for translation, our data show that the amyloid core is exposed for interaction with ACI-6677 as demonstrated by the efficient inhibition of spreading in a mouse model of TDP-43 proteinopathy.

The animal model used in this study was selected to mimic the formation and spreading of phosphorylated TDP-43 inclusions, the unique molecular neuropathology hallmark of TDP-43 proteinopathies in patients that is correlated with the clinical progression of disease [7, 17]. Unfortunately, the model has certain limitations as behavioural readouts are similar whether hTDP-43 transcript is expressed or not and thus, are not suitable for evaluation [14]. In addition to spreading in the extracellular space, other mechanisms for spreading of TDP-43 pathology have been described in disease models such as cell-to-cell transfer of pathological species by tunnelling nanotubes and extracellular vesicles [12, 15]. However, since the relative contribution of each of these mechanism remains unclear, clinical evaluation of targeting each mechanism individually is needed.

Importantly, binding of ACI-6677 in the amyloid core region efficiently neutralized the seeding activity of TDP-43 to inhibit spreading of pathology from ipsilateral to the contralateral side. The mechanism of action of TDP-43 immunotherapy potentially involves two non-exclusive mechanisms to prevent spreading of pathology by efficient neutralization as well as clearance of extracellular TDP-43 species. The data from the *in vitro* studies presented here demonstrate that ACI-6677 efficiently binds and neutralizes the aggregation property of TDP-43. Moreover, the study with microglial uptake demonstrates an increased phagocytic capacity of the immune cells in the presence of the immune complexes as compared to TDP-43 aggregates alone reinforcing the importance of the Fc effector function for clearance afforded by a mAb [1]. In conclusion, these data demonstrate for the first time that an immunotherapy approach was able to reduce spreading of TDP-43 neuropathology in a mouse model providing hope of translating to disease amelioration in patients.

Conclusions

TDP-43 spreading and seeding in the central nervous system is crucial in the clinical progression of ALS and FTD. Our findings reinforce the role of TDP-43 C-terminal fragments comprising the amyloid core region and contributing to spreading and seeding of pathology. By identification of a new mAb binding in the TDP-43 amyloid core, our findings demonstrate for the

first time that an antibody can neutralize seeding-competent TDP-43 in an animal model of disease and thus reduce spreading of TDP-43 neuropathology. It confirms the relevance of targeting extracellular pathogenic TDP-43 by passive immunotherapy. These findings also explain the efficacy of other reported immunotherapies binding in or distal to the amyloid core region of TDP-43 [1, 32]. Finally, the availability of a mAb binding in the amyloid core of TDP-43 opens new research avenues to obtain not only mechanistic insights into the pathobiology of TDP-43 C-terminal fragments but also implement new criteria for disease stratification. Altogether, the preclinical data reported here provides additional support for ongoing drug development programs testing the potential therapeutic benefit of molecules directed against the C-terminal region of TDP-43.

Abbreviations

AD	Alzheimer's disease
ALS	Amyotrophic lateral sclerosis
ANOVA	Analysis of variance
CE-SDS	Capillary electrophoresis sodium dodecyl sulphate
CamKIIa	Calcium/calmodulin dependent protein kinase II alpha
CTE	Chronic traumatic encephalopathy
DAPI	4',6-Diamidino-2-phenylindol
DN	Dystrophic neurites
DTT	Dithiothreitol
EC ₅₀	Half maximal effective concentration
EDC	1-Ethyl-3-(3-dimethylaminopropyl) carbodiimide
ELISA	Enzyme linked immunosorbent assay
FITC	Fluorescein isothiocyanate
FL	Full length
FTLD-TDP	Frontotemporal lobar degeneration with TDP-43 pathology
GCU	Green calibrated unit
IACUC	Institutional animal care and use committee
IBM	Inclusion body myositis
IF	Immunofluorescence
i.p.	Intraperitoneal
K _D	Binding constant
LATE	Limbic-predominant age-related TDP-43 encephalopathy
LCD	Low complexity domain
mAb	Monoclonal antibody
MBP	Maltose binding protein
MW	Molecular weight
mpi	Months post injection
NCA	Non compartmental analysis
NCI	Neuronal cytoplasmic inclusions
NHS	N-hydroxysuccinimide
NLSm	Mutated nuclear localization signal
nsTEM	Negative stain transmission electron microscopy
OCT	Optimal cutting temperature
PD	Parkinson's disease
PFA	Paraformaldehyde
pNPP	Para-nitrophenyl phosphate
PK	Pharmacokinetics
RRM	RNA recognition motif
ROI	Region of interest
RT	Room temperature
SEM	Standard error of the mean
SD	Standard deviation
SPR	Surface plasmon resonance
TEV	Tobacco etch virus
TDP-43	Transactive response DNA binding protein of 43 kDa

Supplementary Information

The online version contains supplementary material available at <https://doi.org/10.1186/s40478-024-01867-z>.

Supplementary Material 1.

Acknowledgements

We would like to thank Prof. Virginia Lee and Dr. Silvia Porta for providing expert opinion in the setting up of the mouse model. We thank Kristina Deduck and Barry Bedell from Biospective (Canada) for performing the in vivo experiments. We thank Florian Udry, Paula Stephen and Bojana Portmann for constructive feedback on the manuscript. We thank Prof. William Seeley and Neurodegenerative Disease Brain Bank UCSF (funding support from NIH grants P01AG019724 and P50AG023501, the Consortium for Frontotemporal Dementia Research, and the Tau Consortium); Netherlands Brain Bank, Netherlands Institute for Neuroscience, Amsterdam; Prof. Tammaryn Lashley and Queen Square Brain Bank for Neurological Disorders, UCL.

Author contributions

M.K., A.P., T.S. and T.A. conceived the study. E.C., M.A., M.R., R.O., A.F., K.P. contributed to the experiments in design, execution, and interpretation. E.C., T.S., M.K. and T.A. wrote the manuscript.

Funding

This study was funded by AC Immune SA.

Availability of data and materials

All data associated with this study are in the paper or the Supplementary Materials.

Declarations

Ethics approval and consent to participate

Informed consent for autopsy and usage of tissue for research purposes had been obtained from probands or their legal representative in accordance with local institutional review boards. All animal procedures were performed according to institutional guidelines approved by respective country's governmental ethics committee.

Consent for publication

Not applicable.

Competing interests

T.A. and T.S. are coinventors on a patent application, publication number WO2020/234473. R.O., T.A. and T.S. are coinventors on a patent application, publication number WO2022/034228. E.C., M.R., R.O., A.F., K.P., A.P., M.V., T.S. are employees of AC Immune and entitled to options and/or shares. M.A. and T.A. were employee of AC Immune at the time of this study. The other authors declare no competing interests.

Received: 30 April 2024 Accepted: 23 September 2024

Published online: 03 October 2024

References

1. Afroz T, Chevalier E, Audrain M, Dumayne C, Ziehm T, Moser R et al (2023) Immunotherapy targeting the C-terminal domain of TDP-43 decreases neuropathology and confers neuroprotection in mouse models of ALS/FTD. *Neurobiol Dis* 179:106050. <https://doi.org/10.1016/j.nbd.2023.106050>
2. Afroz T, Perez-Berlanga M, Polymenidou M (2019) Structural transition, function and dysfunction of TDP-43 in neurodegenerative diseases. *Chimia (Aarau)* 73:380–390. <https://doi.org/10.2533/chimia.2019.380>
3. Arai T, Hasegawa M, Akiyama H, Ikeda K, Nonaka T, Mori H et al (2006) TDP-43 is a component of ubiquitin-positive tau-negative inclusions in frontotemporal lobar degeneration and amyotrophic lateral sclerosis.

- Biochem Biophys Res Commun 351:602–611. <https://doi.org/10.1016/j.bbrc.2006.10.093>
4. Arseni D, Chen R, Murzin AG, Peak-Chew SY, Garringer HJ, Newell KL et al (2023) TDP-43 forms amyloid filaments with a distinct fold in type A FTLD-TDP. *Nature* 620:898–903. <https://doi.org/10.1038/s41586-023-06405-w>
 5. Arseni D, Hasegawa M, Murzin AG, Kametani F, Arai M, Yoshida M et al (2021) Structure of pathological TDP-43 filaments from ALS with FTLD. *Nature*. <https://doi.org/10.1038/s41586-021-04199-3>
 6. Audrain M, Egesipe AL, Tentillier N, Font L, Ratnam M, Mottier L et al (2023) Targeting amyotrophic lateral sclerosis by neutralizing seeding-competent TDP-43 in CSF. *Brain Commun* 5:fcad306. <https://doi.org/10.1093/braincomms/fcad306>
 7. Bretschneider J, Del Tredici K, Toledo JB, Robinson JL, Irwin DJ, Grossman M et al (2013) Stages of pTDP-43 pathology in amyotrophic lateral sclerosis. *Ann Neurol* 74:20–38. <https://doi.org/10.1002/ana.23937>
 8. Buratti E (2018) TDP-43 post-translational modifications in health and disease. *Expert Opin Ther Targets* 22:279–293. <https://doi.org/10.1080/14728222.2018.1439923>
 9. Chornenkyy Y, Fardo DW, Nelson PT (2019) Tau and TDP-43 proteinopathies: kindred pathologic cascades and genetic pleiotropy. *Lab Invest* 99:993–1007. <https://doi.org/10.1038/s41374-019-0196-y>
 10. Cohen TJ, Hwang AW, Restrepo CR, Yuan CX, Trojanowski JQ, Lee VM (2015) An acetylation switch controls TDP-43 function and aggregation propensity. *Nat Commun* 6:5845. <https://doi.org/10.1038/ncomms6845>
 11. Conicella AE, Zerze GH, Mittal J, Fawzi NL (2016) ALS mutations disrupt phase separation mediated by alpha-helical structure in the TDP-43 low-complexity C-terminal domain. *Structure* 24:1537–1549. <https://doi.org/10.1016/j.str.2016.07.007>
 12. Ding X, Ma M, Teng J, Teng RK, Zhou S, Yin J et al (2015) Exposure to ALS-FTD-CSF generates TDP-43 aggregates in glioblastoma cells through exosomes and TNTs-like structure. *Oncotarget* 6:24178–24191. <https://doi.org/10.18632/oncotarget.4680>
 13. Gasset-Rosa F, Lu S, Yu H, Chen C, Melamed Z, Guo L et al (2019) Cytoplasmic TDP-43 de-mixing independent of stress granules drives inhibition of nuclear import, loss of nuclear TDP-43, and cell death. *Neuron* 102(339–357):e337. <https://doi.org/10.1016/j.neuron.2019.02.038>
 14. Igaz LM, Kwong LK, Lee EB, Chen-Plotkin A, Swanson E, Unger T et al (2011) Dysregulation of the ALS-associated gene TDP-43 leads to neuronal death and degeneration in mice. *J Clin Invest* 121:726–738. <https://doi.org/10.1172/JCI44867>
 15. Iguchi Y, Eid L, Parent M, Soucy G, Bareil C, Riku Y et al (2016) Exosome secretion is a key pathway for clearance of pathological TDP-43. *Brain* 139:3187–3201. <https://doi.org/10.1093/brain/aww237>
 16. Karanth S, Nelson PT, Katsumata Y, Kryscio RJ, Schmitt FA, Fardo DW et al (2020) Prevalence and clinical phenotype of quadruple misfolded proteins in older adults. *JAMA Neurol*. <https://doi.org/10.1001/jamaneurol.2020.1741>
 17. Kawakami I, Arai T, Hasegawa M (2019) The basis of clinicopathological heterogeneity in TDP-43 proteinopathy. *Acta Neuropathol* 138:751–770. <https://doi.org/10.1007/s00401-019-02077-x>
 18. Kouhi A, Pachipulusu V, Kapenstein T, Hu P, Epstein AL, Khawli LA (2021) Brain disposition of antibody-based therapeutics: dogma, approaches and perspectives. *Int J Mol Sci* 22:6442. <https://doi.org/10.3390/ijms22126442>
 19. Kumar ST, Nazarov S, Porta S, Maharjan N, Cendrowska U, Kabani M et al (2023) Seeding the aggregation of TDP-43 requires post-fibrillization proteolytic cleavage. *Nat Neurosci* 26:983–996. <https://doi.org/10.1038/s41593-023-01341-4>
 20. Kwong LK, Irwin DJ, Walker AK, Xu Y, Riddle DM, Trojanowski JQ et al (2014) Novel monoclonal antibodies to normal and pathologically altered human TDP-43 proteins. *Acta Neuropathol Commun* 2:33. <https://doi.org/10.1186/2051-5960-2-33>
 21. Laferriere F, Maniecka Z, Perez-Berlanga M, Hruska-Plochan M, Gilhespy L, Hock EM et al (2019) TDP-43 extracted from frontotemporal lobar degeneration subject brains displays distinct aggregate assemblies and neurotoxic effects reflecting disease progression rates. *Nat Neurosci* 22:65–77. <https://doi.org/10.1038/s41593-018-0294-y>
 22. Lee EB, Porta S, Michael Baer G, Xu Y, Suh E, Kwong LK et al (2017) Expansion of the classification of FTLD-TDP: distinct pathology associated with rapidly progressive frontotemporal degeneration. *Acta Neuropathol* 134:65–78. <https://doi.org/10.1007/s00401-017-1679-9>
 23. Maurel C, Chami AA, Thepault RA, Marouillat S, Blasco H, Corcia P et al (2020) A role for SUMOylation in the formation and cellular localization of TDP-43 aggregates in amyotrophic lateral sclerosis. *Mol Neurobiol* 57:1361–1373. <https://doi.org/10.1007/s12035-019-01810-7>
 24. McKee AC, Gavett BE, Stern RA, Nowinski CJ, Cantu RC, Kowall NW et al (2010) TDP-43 proteinopathy and motor neuron disease in chronic traumatic encephalopathy. *J Neuropathol Exp Neurol* 69:918–929. <https://doi.org/10.1097/NEN.0b013e3181ee7d85>
 25. Nelson PT, Dickson DW, Trojanowski JQ, Jack CR, Boyle PA, Arfanakis K et al (2019) Limbic-predominant age-related TDP-43 encephalopathy (LATE): consensus working group report. *Brain* 142:1503–1527. <https://doi.org/10.1093/brain/awz099>
 26. Neumann M (2009) Molecular neuropathology of TDP-43 proteinopathies. *Int J Mol Sci* 10:232–246. <https://doi.org/10.3390/ijms10010232>
 27. Neumann M, Kwong LK, Lee EB, Kremmer E, Flatley A, Xu Y et al (2009) Phosphorylation of S409/410 of TDP-43 is a consistent feature in all sporadic and familial forms of TDP-43 proteinopathies. *Acta Neuropathol* 117:137–149. <https://doi.org/10.1007/s00401-008-0477-9>
 28. Neumann M, Sampathu DM, Kwong LK, Truax AC, Micsenyi MC, Chou TT et al (2006) Ubiquitinated TDP-43 in frontotemporal lobar degeneration and amyotrophic lateral sclerosis. *Science* 314:130–133. <https://doi.org/10.1126/science.1134108>
 29. Nonaka T, Masuda-Suzukake M, Arai T, Hasegawa Y, Akatsu H, Obi T et al (2013) Prion-like properties of pathological TDP-43 aggregates from diseased brains. *Cell Rep* 4:124–134. <https://doi.org/10.1016/j.celrep.2013.06.007>
 30. Porta S, Xu Y, Lehr T, Zhang B, Meymand E, Olufemi M et al (2021) Distinct brain-derived TDP-43 strains from FTLD-TDP subtypes induce diverse morphological TDP-43 aggregates and spreading patterns in vitro and in vivo. *Neuropathol Appl Neurobiol* 47:1033–1049. <https://doi.org/10.1111/nan.12732>
 31. Porta S, Xu Y, Restrepo CR, Kwong LK, Zhang B, Brown HJ et al (2018) Patient-derived frontotemporal lobar degeneration brain extracts induce formation and spreading of TDP-43 pathology in vivo. *Nat Commun* 9:4220. <https://doi.org/10.1038/s41467-018-06548-9>
 32. Riemenschneider H, Simonetti F, Sheth U, Katona E, Roth S, Hutten S et al (2023) Targeting the glycine-rich domain of TDP-43 with antibodies prevents its aggregation in vitro and reduces neurofilament levels in vivo. *Acta Neuropathol Commun* 11:112. <https://doi.org/10.1186/s40478-023-01592-z>
 33. Salajegheh M, Pinkus JL, Taylor JP, Amato AA, Nazareno R, Baloh RH et al (2009) Sarcoplasmic redistribution of nuclear TDP-43 in inclusion body myositis. *Muscle Nerve* 40:19–31. <https://doi.org/10.1002/mus.21386>
 34. Seyfried NT, Gozal YM, Dammer EB, Xia Q, Duong DM, Cheng D et al (2010) Multiplex SILAC analysis of a cellular TDP-43 proteinopathy model reveals protein inclusions associated with SUMOylation and diverse polyubiquitin chains. *Mol Cell Proteomics* 9:705–718. <https://doi.org/10.1074/mcp.M800390-MCP200>
 35. Tamaki Y, Ross JP, Alipour P, Castonguay CE, Li B, Catoire H et al (2023) Spinal cord extracts of amyotrophic lateral sclerosis spread TDP-43 pathology in cerebral organoids. *PLoS Genet* 19:e1010606. <https://doi.org/10.1371/journal.pgen.1010606>
 36. Tsuji H, Arai T, Kametani F, Nonaka T, Yamashita M, Suzukake M et al (2012) Molecular analysis and biochemical classification of TDP-43 proteinopathy. *Brain* 135:3380–3391. <https://doi.org/10.1093/brain/aww230>
 37. Young AL, Vogel JW, Robinson JL, McMillan CT, Ossenkoppele R, Wolk DA et al (2023) Data-driven neuropathological staging and subtyping of TDP-43 proteinopathies. *Brain* 146:2975–2988. <https://doi.org/10.1093/brain/awad145>

Publisher's Note

Springer Nature remains neutral with regard to jurisdictional claims in published maps and institutional affiliations.